Increasing Isoprene Epoxydiol-to-Inorganic Sulfate Aerosol (IEPOX:$Sulf_{inorg}$) Ratio Results in Extensive Conversion of Inorganic Sulfate to Organosulfur Forms: Implications for Aerosol Physicochemical Properties

Matthieu Riva[†,#,¥,*], Yuzhi Chen[†,¥], Yue Zhang[†,§], Ziying Lei[ǁ], Nicole E. Olson[⊥], Hallie C. Boyer[#], Shweta Narayan[#], Lindsay D. Yee[∇], Hilary S. Green[†,‡], Tianqu Cui[†], Zhenfa Zhang[†], Karsten Baumann[○], Mike Fort[○], Eric Edgerton[○], Sri H. Budisulistiorini[†,◆], Caitlin A. Rose[†], Igor O. Ribeiro[¶], Rafael L. e Oliveira[¶], Erickson O. dos Santos[∞], Cristine M. D. Machado[∞], Sophie Szopa[∏], Yue Zhao[¬,"], Eliane G. Alves[$], Suzane S. de Sá[□], Weiwei Hu[•], Eladio M. Knipping[~], Stephanie L. Shaw[···], Sergio Duvoisin Junior[¶], Rodrigo A. F. de Souza[¶], Brett B. Palm[•], Jose-Luis Jimenez[•], Marianne Glasius[¨], Allen H. Goldstein[∇], Havala O. T. Pye[†,þ], Avram Gold[†], Barbara J. Turpin[†], William Vizuete[†], Scot T. Martin[□,»], Joel A. Thornton[¬], Cari S. Dutcher[#], Andrew P. Ault[ǁ,⊥*], and Jason D. Surratt[†*]

Affiliations:

[†] Department of Environmental Sciences and Engineering, Gillings School of Global Public Health, The University of North Carolina at Chapel Hill, Chapel Hill, NC 27599, USA.

[§] Aerodyne Research Inc., Billerica, MA 01821, USA.

[ǁ] Department of Environmental Health Sciences, University of Michigan, Ann Arbor, MI 48109, USA.

[⊥] Department of Chemistry, University of Michigan, Ann Arbor, MI 48109, USA.

[#] Department of Mechanical Engineering, University of Minnesota-Twin Cities, Minneapolis, MN 55455, USA.

[∇] Department of Environmental Science, Policy, and Management, University of California, Berkeley, CA 94720, USA.

[○] Atmospheric Research & Analysis, Inc., Cary, NC 27513, USA.

[¶] Escola Superior de Tecnologia, Universidade do Estado do Amazonas, Manaus, Amazonas, 69050, Brazil.

[∞] Department of Chemistry, Federal University of Amazonas, Manaus, Amazonas, 69067, Brazil.

[∏] Laboratoire des Sciences du Climat et de l'Environnement, CEA-CNRS-UVSQ-IPSL, 91190, Gif-sur-Yvette, France.

[¬] Department of Atmospheric Sciences, University of Washington, Seattle, WA 98195, USA.

[$] Environment Dynamics Department, National Institute of Amazonian Research (INPA), Manaus, 69067, Brazil.

[□] John A. Paulson School of Engineering and Applied Sciences, Harvard University, Cambridge, MA 02138, USA.

• Department of Chemistry and Cooperative Institute for Research in Environmental Sciences, University of Colorado, Boulder, CO 80309, USA.

~ Electric Power Research Institute, Washington, D.C 20005, USA.

··· Electric Power Research Institute, Palo Alto, CA 94304, USA.

¨ Aarhus University, Dept. of Chemistry and iNANO, 8000 Aarhus C, Denmark.

þ National Exposure Research Laboratory, US Environmental Protection Agency, Research Triangle Park, NC 27711, USA.

» Department of Earth and Planetary Sciences, Harvard University, Cambridge, MA 02138, USA.

This PDF file includes:

Materials and Methods

Collection of $PM_{2.5}$ Collection from SE-U.S. $PM_{2.5}$ samples were collected onto pre-baked 8 × 10 in Tissuquartz™ Filters (Pall Life Sciences) using three high-volume $PM_{2.5}$ samplers (Tisch Environmental) operated at 1 m^3 min^{-1} during the 2013 Southern Oxidant and Aerosol Study (SOAS) campaign from 1 June to 15 July 2013 at the CTR, AL ground site. One high-volume sampler collected $PM_{2.5}$ for 23 h (08:00 to 07:00 the next day, local time), while the two remaining high-volume samplers followed two cycles. When the sampling schedules were daytime (08:00 – 19:00, local time) and nighttime (20:00 – 07:00, local time), the $PM_{2.5}$ collected were defined as regular day or night samples, respectively. When atmospheric chemical model simulations predicted a high level of BVOCs, sulfate and NO_x[1], $PM_{2.5}$ were collected more frequently (collection times were 08:00–11:00, 12:00–15:00, 16:00–19:00, and 20:00–07:00, local time) in order to examine the potential enhancing effect of anthropogenic pollutants on BSOA formation, and are defined as "intensive" samples. Field blanks were also collected weekly by placing pre-baked quartz filters into the 3 non-operating high-volume $PM_{2.5}$ samplers for 15 min. Filters and field blanks were stored under dark conditions at –20ºC until analysis.

Collection of $PM_{2.5}$ Samples from Central Amazonia (Manaus downtown). $PM_{2.5}$ samples were collected daily from 18 July through 1 August 2016 on filters similar to those used during the SOAS campaign using a high-volume $PM_{2.5}$ sampler operated at 1.13 m^3 min^{-1}. The sampling site was located at 6 m above the ground at the School of Technology of the State University of Amazonas in Manaus, Brazil. The high-volume $PM_{2.5}$ sampler was flow-calibrated and the filter holder was cleaned with the filter extraction solvent each day before sampling to ensure no chemical carryover between samples. All filters were collected for 24 h. Immediately after collection, the 15 daily $PM_{2.5}$ filter samples were stored at –18 ºC under dark conditions until chemical analysis. One field blank was collected during the 15-day campaign by placing a pre-baked quartz filter into the high-volume $PM_{2.5}$ sampler for 15 min, and then removing and storing it under the same conditions as the field samples. Co-located measurements of total organic and inorganic aerosol mass were not available for Manaus and the contribution of the OS could not be calculated.

Collection of PM_1 Samples from downwind Manaus. Filters were collected during the Green Ocean Amazon (GoAmazon2014/5) field campaign[2] during intensive operating period 2 (IOP2) at the T3 site ~ 70 km downwind of Manaus in August-October of 2014. The prevailing wind direction is from north-east, transporting air masses over the Amazon forest to be mixed with the outflow from Manaus (to the east) before reaching the sampling site. Transport time from city to T3 site was typically 4-5 h.[3]

Aerosol samples (PM_1) were collected on quartz fiber filters (101.6 mm diameter, QM-A Quartz, Whatman) using a custom-built sequential filter sampler (Aerosol Dynamics, Inc.). Air was sampled 4 m above ground level, passed through tubing kept at temperatures below the dew point for trapping excess water, and then through a greaseless cyclone (with a 1 μm aerodynamic diameter cut-point), before collection of particles. Filters were pre-treated by baking at 550°C for 12 hours. While samples were collected with a 4-hour time resolution, 24-h average data are presented in this study. Field blanks were collected each week by inserting pre-baked filters (same filters used for actual sample collection) into the filter holders for at least a minute, and then removing following the same procedures as it is with field samples. Particle and blank filters were kept frozen (–18°C) and transported on ice.

Chemical Characterization

Filter Extraction and Chemical Analysis of OS. Chemical characterization of the $PM_{2.5}$ samples was performed by UPLC/ESI-HR-Q-TOFMS (6520 Series, Agilent) in the negative ion mode, under operating conditions described in detail elsewhere [4,5]. High-volume quartz filter 37 mm punches were extracted with 22 mL of high-purity methanol (LC-MS CHROMASOLV-grade, Sigma-Aldrich) by sonication for 45 min, filtered through 0.2-μm PTFE syringe filters (Pall Life Science, Acrodisc) to remove insoluble particles or quartz filter fibers and blown dry under a gentle N_2 (g) stream at ambient temperature. The dried extracts were reconstituted with 150 μL of a 50:50 (v/v) solvent mixture of methanol (LC-MS CHROMASOLV-grade, Sigma-Aldrich) and high-purity water (Milli-Q, 18.2 M). Five μL aliquots were injected onto the UPLC column (Waters ACQUITY UPLC HSS T3 column, 2.1 × 100 mm, 1.8 μm particle size) and eluted at a flow rate of 0.3 mL min^{-1} with a solvent mixture of methanol containing 0.1% acetic acid (LC-MS

105 CHROMASOLV-grade, Sigma-Aldrich) and water containing 0.1% acetic acid (LC-MS CHROMASOLV-
106 grade, Sigma-Aldrich).

107 Field, lab and blank filters from CTR, were spiked with known amounts of propyl and octyl sulfate
108 (electronic grade, City Chemical LLC) to estimate the extraction efficiency and potential losses throughout
109 the analytical protocol. Neither of these two OS have been identified in atmospheric $PM_{2.5}$, and thus can be
110 used as internal standards. Recovery was determined to be 89 ± 14 (1 std. dev.) %. To estimate potential
111 losses of MSA, control experiments were performed by analyzing five prebaked filters spiked with a known
112 amount of MSA. Extraction efficiency was above 70% and was used to correct the quantification of
113 samples. To optimize the quantification of identified BVOC-derived OS, a mixture of IEPOX-OS
114 ($C_5H_{11}O_7S^-$)[1], 2-methylglyceric acid sulfate ($C_4H_7O_7S^-$)[6] and 2-oxopropyl sulfate ($C_3H_5O_5S^-$)[7] were
115 synthesized in-house as authentic standards. Propyl sulfate ($C_3H_7O_4S^-$; electronic grade, City Chemical
116 LLC) and 3-pinanol-2-hydrogen sulfate ($C_9H_{13}O_6S^-$; synthesized standard) served as surrogate standards to
117 quantify the remaining OS. Surrogate standards were selected to match as precisely as possible the retention
118 times of the compounds of interest, as summarized in Tables S2-S4. Due to the potential influence of marine
119 air masses at the CTR site, methanesulfonic acid formed from the oxidation of dimethyl sulfide [8] was also
120 quantified in all $PM_{2.5}$ samples from CTR using an authentic standard (MSA, Sigma Aldrich, ≥ 99.5%) to
121 help with mass closure of total organosulfur compounds.

122 PILS vials were analyzed by UPLC/ESI-HR-Q-TOFMS operated in negative mode following the
123 analytical procedure described for the ambient filter extracts. PILS vials were analyzed for the data
124 presented in the main text (Figure 1) in order to provide time-resolved information for the conversion of
125 SO_4^{2-} to organosulfur forms.

126 ***PILS Operation and Dilution Correction.*** The aerosols are sampled through an impactor with a 2.5-μm
127 cut-off at a flow rate of ~ 13 L min^{-1} with a carbon strip denuder (Sunset Labs) upstream of the impactor to
128 remove organic vapor. Cool sample air flow was mixed adiabatically with a steam heated at 98.5-100℃ in
129 the PILS condensation chamber, which allows aerosol particles to grow sufficiently for collection on a

quartz impactor plate. Impacted droplets were transferred by a wash-flow at 0.50 – 0.55 mL min^{-1} into a debubbler and the resulting bubble-free sample liquid was delivered through a tubing with an inline filter into 2 mL glass vials in a rotating-carousel auto-collector (BMI). Air sampling rate and wash-flow rate were checked and recorded before and after each experiment. Milli-Q water used in the wash-flow was spiked with 25 μM of lithium bromide (LiBr) as an internal standard to correct for dilution caused by condensation of water vapor during droplet collection inside the PILS. Ideally the concentrations of lithium bromide in the samples should be identical to that in the wash-flow supply bottle without dilution. When taking into account the addition of water due to condensations, the dilution factor can be calculated on a per sample basis using bromide ion concentration measured by IC as such:

$$\text{dilution factor} = \frac{[Br^-]_{wash}}{[Br^-]_i}$$

In this equation, subscript "i" denotes bromide concentration measured in each sample and subscript "wash" denotes the bromide concentration measured for the liquid in the wash-flow supply bottle. Then the correction was made for all SOA tracers in a sample by multiplying the measured tracer concentrations by the dilution factor derived above.

Uncertainty Estimates for OS. The use of surrogate standards can lead to significant biases in the OS quantification. The ESI can be highly impacted by the chemical composition of the mobile phase; for example, when increasing the organic content of the eluent, the ionization efficiency increases significantly [9]. As presented Table S5, calibration factors were determined for several authentic OS standards to evaluate the impact of the chemical structure as well as the mobile phase composition on the ionization efficiency of the compounds of interest. During the first two minutes of the gradient elution, the mobile phase is composed 100% water, and therefore effect of solvent composition on ionization efficiency is not expected within this time period. We note that most of the isoprene-derived OS eluted within the first two minutes and sensitivities towards standards eluting within this period are independent of structure. This suggests that uncertainties in quantification using the surrogate standards for OS eluting in this time range are most

likely small (< 10%). For the later eluting compounds (e.g. monoterpene-derived OS) the composition of the mobile phase changes and could impact the ionization efficiency. Propyl sulfate and 3-pinanol-2-hydrogen sulfate were used as surrogate standards and selected to correspond as precisely as possible to the retention times of the OS identified in the SOA collected during SOAS. Although the sensitivities of propyl and 3-pinanol-2-hydrogen sulfates are of the same order, biases can be expected and might lead to an inaccurate estimation of the concentration of the OS eluting later in the run.

We assume a small uncertainty in the calibration curve itself (5%). Uncertainties from the extraction based on the recovery of propyl and octyl sulfates are 15%. In addition to extraction efficiencies and calibration uncertainties, uncertainty related to the volume of air sampled could further contribute to overall uncertainty. In the different campaigns, high-volume samplers were calibrated and the air volumes adjusted based on the meteorological conditions. Therefore, this uncertainty was estimated as 5%. Overall uncertainty in quantification is estimated to be ±17%.

Characterization of Total Water-Soluble Organosulfur at CTR. Total water-soluble organosulfur compound mass present in SOA collected in the SE-U.S. was determined from the difference between total water-soluble sulfur measured by isotope ratio inductively coupled plasma mass spectrometry (IR-ICP-MS) and sulfate-sulfur measured by ion chromatography (IC) in the same sample aliquot. Sample extractions, sample spiking and standard preparation were performed gravimetrically, using a 5-place readout laboratory balance (Mettler Toledo Model MS205DU). High-volume quartz filter punches (47 mm, or 37 mm diameter) were extracted in Thermo-Fisher Nalgene wide mouth lab quality HDPE bottles (1 oz. 02-893-5A) with 25 g distilled deionized water (DIW with 18.2 ± 0.2 MΩcm resistivity). Each vessel was capped by a polypropylene cap and sonicated without heat for 1 h. After sonication, the sample was allowed to cool, shaken for uniformity, and allowed to equilibrate at 8^{o}C overnight.

Each extract was analyzed in triplicate for sulfate via IC using a dual-channel Dionex ICS-3000 ion chromatography system and Dionex AS-1 Autosampler. The IC was calibrated with NIST SRM 3181 (sulfate in water) at concentrations between 10 ngS g^{-1} and 2,000 ngS g^{-1}. A gradient profile (5mM-30mM)

of KOH was used as eluent for sulfate-S separation (MSA for cations in other channel) with 4 micro-bore IonPac analytical column AS18 (CS16 for cations). Each channel operated a self-regenerating SRS-ULTRA suppressor in external DIW regeneration mode, a CD-1 conductivity detector, and a DP-1/SP-1 gradient pump with built-in degassing. The applied micro-bore system allowed an analyte flow rate of 1 mL min^{-1}. DIW was supplied directly to the eluent generator module. The instrument detection limit (IDL) for the sulfate anion expressed in ambient concentrations from field blanks amounts to less than 2 ngS m^{-3}. Average precision determined from triplicate analysis of the samples collected during the study is 0.46 ± 0.40%. Secondary source standards were used to routinely assess accuracy in terms of recovery, which averages 99.6 ± 0.4%.

Each extract was also analyzed in triplicate for total-S using a Perkin Elmer ELAN DRC-II IR-ICP-MS operated in Dynamic Reaction Cell (DRC) mode with oxygen reaction gas (UHP 99.999% O_2, Airgas, 4808 Nelson Rd. Morrisville, NC 27560). The IR-ICP-MS was calibrated with NIST SRM 3181 at concentrations between 100 ngS g^{-1} and 2000 ngS g^{-1}. Standards and sample aliquots were spiked with $Na_2{}^{33}SO_4$ (Sigma-Aldrich cat. # 719374) to a final concentration of approximately 1000 ng^{33}S g^{-1} and then analyzed for ^{32}SO (48amu), ^{33}SO (49amu) and ^{34}SO (50amu). Total water-soluble S was calculated as follows:

$$\text{Total-S [ngS g}^{-1}\text{]} = (^{32}\text{SO}/\,^{33}\text{SO})_{sa} * [^{33}\text{SO}]_{sp} / IR_{48/49}$$

with ^{32}SO and ^{33}SO = background-corrected counts at 48 amu and 49 amu, respectively; sa = sample; sp = spike concentration [ngS g^{-1}]; $IR_{48/49}$= ion intensity ratio for masses 48 and 49. The instrument detection limit of the IR-ICP-MS can be estimated conservatively at 2 ngS g^{-1} or 50 ngS^{-1} per sample, translating to less than 2 ngS m^{-3} atmospheric $PM_{2.5}$ concentration of total water-soluble S. Average precision for triplicate analysis of samples was 0.35 ± 0.20%. Recoveries of a secondary sulfate standard (10,000 μgS mL^{-1} ± 0.5%, 10M54-5 from HP Standards, Charleston, SC) were 100.3 ± 0.4%, and recoveries of camphorsulfonic acid (CSA), methanesulfonic acid (MSA) and methionine were 99.9 ± 0.3%, 98.9 ± 0.3% and 98.2 ± 0.2%, respectively (purity of CSA and MSA was 99% from ACROS Organics via Fisher-Scientific, purity of

methionine was >98.5% from Fisher BioReagents). All recovery checks were run at a 10% frequency or every 10 samples.

Based on the above results (in particular the 0.16% uncertainty in the NIST SRM 3181, the linearity of the IC and IR-ICP-MS calibrations, and the instruments' recoveries of the secondary standards), the approximate 95% (σ=2) uncertainty for the difference between total-S and sulfate-S is ± 1.6 %. In other words, water-soluble organosulfur compounds are greater than 0 at the 95% confidence level when total-S via IR-ICP-MS is at least 1.6% greater than sulfate-S via IC.

Uncertainty Estimates for Water Soluble Sulfate-S by IC and Water Soluble Total-S by ICP-MS.

Sulfate-S via Ion Chromatography

The mass of sulfate-S in a sample extract is determined as shown in eqn. 1.

$$\text{Sulfate-S(ng)} = \text{Sulfate-S(ng-g}^{-1}\text{)} * \text{Extract Mass (g)} \quad (1)$$

The uncertainty (U) in Sulfate-S can then be estimated as shown in eqn. 2

$$U_{\text{Sulfate-S}} = ((\mu_{\text{Sulfate-S}})^2 + (\mu_{\text{Extract Mass}})^2)^{1/2} \quad (2)$$

Which can be expanded to

$$U_{\text{Sulfate-S}}\,(\%) = 100\%*((\mu_{\text{Primary}})^2 + (\mu_{\text{Secondary}})^2 + (\mu_{\text{Rep}})^2 + (\mu_{\text{Dilution}})^2 + (\mu_{\text{Extract Mass}})^2)^{1/2} \quad (3)$$

Where,

$\boldsymbol{\mu_{\text{Primary}}}$ = relative uncertainty in the primary sulfate standard (NIST SRM 3181) = 0.0016, from NIST certificate.

$\boldsymbol{\mu_{\text{Secondary}}}$ = relative recovery of the secondary sulfate standard = 0.0039, measured.

$\boldsymbol{\mu_{\text{Rep}}}$ = relative standard deviation of sample replicates = 0.0046, measured.

$\boldsymbol{\mu_{\text{Dilution}}}$ = relative standard deviation of primary standard diluent mass = 0.0003, based on balance uncertainty of +/- 10 mg for 30 g standard.

$\boldsymbol{\mu_{\text{Extract Mass}}}$ = relative standard deviation of extract mass = 0.0003, based on balance uncertainty of +/- 10 mg for 30 g sample extract.

Estimated $U_{\text{Sulfate-S}}$ = 0.60%

Total water-soluble S (Total-S) via isotope ratio ICP-MS

The mass of Total-S in a sample extract is determined as shown in eqn. 4.

$$\text{Total-S(ng)} = \text{Total-S(ng-g}^{-1}\text{)} * \text{Extract Mass(g)} \quad (4)$$

$$= ({}^{32}\text{SO}/{}^{33}\text{SO})_{sa} * [{}^{33}\text{S}]_{sp} / IR_{48/49} * \text{Extract Mass} \quad (5)$$

Where,

$({}^{32}\text{SO}/{}^{33}\text{SO})_{sa}$ = ratio of background-corrected counts at 48 amu and 49 amu

$[{}^{33}\text{S}]_{sp}$ = concentration of ^{33}S in the spiked sample

$IR_{48/49}$ = ion ratio for 48 amu and 49 amu (counts per ng-g^{-1}/ counts per ng-g^{-1})

$IR_{48/49}$ is determined by spiking approximately 1000 ngS-g^{-1} of $K_2{}^{33}SO_4$ into solutions of NIST SRM 3181 containing 0, 100, 300, 500, 750, 1000 and 2000 ngS-g^{-1} of total-S. Note that $IR_{48/49}$ decreases by about 1% over the observed calibration range, due to the presence of naturally-occurring ^{33}S in SRM 3181. To partially compensate for decreasing IR, we bin IRs over successive pairs of calibration standards and use the one that brackets an individual sample concentration to calculate Total-S. For example, if the initial estimate of Total-S is between 100 and 300 ng-g^{-1}, we use the average of IRs obtained at calibration levels 100 and 300 ngS-g^{-1}.

The overall procedure assumes that the isotopic composition of SRM 3181 is at least roughly equal to that of naturally-occurring sulfur (and, by inference, ambient samples). To confirm this, we asked a third-party laboratory to measure del^{34}S on a subsample of SRM 3181. Results showed del^{34}S of +17 parts per thousand, relative to Canyon Diablo Troilite. The del^{33}S should be similar to this, based on mass dependent fractionation (0.5 times del^{34}S) plus mass independent fractionation (0.6 to 1.0 times del^{34}S). The impact of these enrichments is negligible, so we did not adjust SRM 3181 concentrations.

Based on the above, $U_{Total\text{-}S}$ can be estimated as shown in eqn. 6

$$U_{Total\text{-}S} = 100\%*((\mu_{CP\text{-}3181})^2 + (\mu_{IP\text{-}33S})^2 + (\mu_{CP33S})^2 + (\mu_{IR})^2 + (\mu_{32SO/33SO})^2 + (\mu_{Secondary})^2 + (\mu_{Dilution})^2 + (\mu_{Spike\ Mass})^2 + (\mu_{Extract\ Mass})^2)^{1/2} \quad (6)$$

Where,

$\boldsymbol{\mu_{CP\text{-}3181}}$ = chemical purity of SRM 3181 = 0.004 (manufacturer's certificate).

$\mu_{IP\text{-}33S}$ = isotopic purity of ^{33}S standard = 0.0013 (ARA analysis of high concentration solutions).

μ_{CP33S} = chemical purity of ^{33}S standard, pooled relative standard deviation of for sulfate, CSA, MSA and methionine = 0.006.

μ_{IR} = relative standard deviation of IR across full calibration curve = 0.0034.

$\mu_{32SO/33SO}$ = relative standard deviation of triplicate sample analyses = 0.0035.

$\mu_{Secondary}$ = relative standard deviation of secondary SO_4 standard recoveries = 0.0042.

$\mu_{Dilution}$ = relative standard deviation of primary standard diluent mass = 0.0003, based on balance uncertainty of +/- 10 mg for 30 g standard.

$\mu_{Spike\ Mass}$ = relative standard deviation of primary standard diluent mass = 0.0016, based on balance uncertainty of +/- 10 mg and 6 g sample aliquot.

$\mu_{Extract\ Mass}$ = relative standard deviation of extract mass = 0.0003, based on balance uncertainty of +/- 10 mg for 30 g sample extract.

Estimated $U_{Total\text{-}S}$ = 0.99%.

Combining $U_{Sulfate\text{-}S}$ and $U_{Total\text{-}S}$ and applying a coverage factor (k) of 2 yields an estimated uncertainty for the difference between Total-S and Sulfate-S of 2.3%, with a confidence interval ≥ 75%.

Microscopy Imaging. A 3-stage microanalysis particle sampler (MPS-3, California Measurements, Inc.) with size cuts of 5.0, 2.5, and 0.4 μm was operated at 2.1 L min^{-1}. Particles were impacted onto carbon-type-b Formvar-coated copper transmission electron microscopy (TEM) grids and silicon wafer substrates (Ted Pella, Inc.). Samples were stored in sealed plastic vials at room temperature prior to analysis. Particles collected onto silicon substrates were imaged in 5x5 μm regions by an AFM (Anasys Instruments) in tapping mode with 75 ± 15 kHz resonant frequency and 1-7 N m^{-1} spring constant at ambient laboratory temperature (~23 °C), pressure, and RH (~36%). SEM analysis of particles collected onto TEM grids was performed by a FEI Helios 650 Nanolab-Dualbeam electron microscope equipped with a high angle annular dark field (HAADF) detector operated at an accelerating voltage of 10.0 kV and a current of 0.80 nA under vacuum conditions (10^{-3} to 10^{-5} Pa). SEM particles were analyzed orthogonal to the beam on TEM grids and at a 55-degree angle (tilted) on the silicon wafer.

Biphasic Microfluidic Experiments with Samples Extracted from Filters. Microfluidic experiments were also conducted with SOA samples (2-MT and IEPOX-OS) extracted from filters using methanol as the solvent. It is observed (Figures S2A and S2B) that methanol itself causes a significant decrease in interfacial tension compared to pure water. Furthermore, similar to the 2-MT and IEPOX-OS samples in water, interfacial tension depression was observed with methanol as the solvent for SOA samples. Figure S2A shows the slight decrease in interfacial tension measured with 2-MT in methanol, compared to the solvent (methanol in water). At 50 mg/mL SOA, IEPOX-OS shows a larger depression in interfacial tension compared to 2-MT (Figure S2B). Finally, when AS is added, significant salting out is observed at 25 mg/mL of IEPOX-OS (Figure S2B).

Isotherm Model for Interfacial Tensions. A surface tension model using adsorption isotherms and based on statistical mechanics was applied to the microfluidic measurements for the 2-MT (Figure S9) and IEPOX-OS compounds (Figure 4A). Traditionally, Langmuir-like isotherm models are applied to surface active organics, such as two parameter Szyszkowski equation (see eq. 1 in Schweir et al.[10] for an example). In the model applied here, unique features of the surface partition function are that the adsorption sites are solvent molecules (waters) and that solutes can occupy a non-integer number of sites using a multifactorial skip, implicitly accounting for the size of the solute. The model expression for binary solutions is $\sigma = \sigma_w - {kT}/{rS_wLn(1 + Ka_s)}$, where r is the surface partition function multifactorial skip, K is a solute bulk energy term, σ_w is the surface tension of pure water, S_w is the area of adsorption sites (the projected area of one water molecule, 0.1 nm^2. The expression was normalized by the interfacial tension value of pure water from biphasic microfluidic tensiometry and subsequently applied to the measurements of 2-MT and IEPOX OS water. The solute bulk energy term (K) follows the expected size-dependence for each compound: K = 47.35 for 2-MT (M_w = 136 g mol^{-1}) and K = 66.00 for IEPOX-OS (M_w = 215 g mol^{-1}). The surface function variable (r) also follows the size-dependence, as r = 71.38 for IEPOX-OS and r = 27.24 for 2-MT. For the salty solutions, the concentrations, or solute activities, were modified using Setschenow constant ($K_s c_{salt} = \log(\gamma/\gamma_0)$, where γ is the organic activity in salty water and γ_0 is the organic activity in pure water. Thus,

306 K_s shows enhancement or depletion of organic surface partitioning due to the presence of salt in solution.
307 An important assumption is that in pure water, the organic activity coefficient is unity at concentrations less
308 than 1.0 mol/L. Incorporating the Setschenow equation into the surface tension equation results in $\sigma = \sigma_w -$
309 $kT/rS_wLn\left(1 + Ka_s * 10^{K_s c_{salt}}\right)$. If parameters *K* and *r* are optimized from the pure water case and interfacial
310 tension is known for the same concentration of organic in both pure water and salty water, then K_s is the
311 single parameter. Recently, Toivola et al. [11] performed quantum chemistry computations of Ks for 2-MT
312 in 0.009 and 0.09 mole fraction of AS and found Ks = 0.568 kg-mol-1 and Ks = 0.866 kg-mol-1,
313 respectively. Our AS mole fraction is 0.03 and we find Ks = 0.299 kg-mol-1 for 2-MT.
314 ***Flow Tube Experiments***. The flow tube, CIMS, as well as aerosol and gas phase IEPOX generation have
315 been described in detail elsewhere.[12] Briefly, the flow tube consists of a 6 x 90 cm Pyrex cylinder having
316 inner walls coated with halocarbon wax to reduce the wall loss of IEPOX gas. ABS aerosol particles were
317 generated using a constant output atomizer (TSI Inc., Model 3076) from dilute solutions (0.1 wt %). The
318 atomizer output was diluted and conditioned to about 38% RH by mixing with a 3 L min^{-1} flow of
319 humidified ultrahigh purity (UHP) N_2 before entering the flow tube. The IEPOX vapor was generated by a
320 flow of 30 standard cubic centimeters per minute (sccm) of UHP N_2 over ~200 μl *trans-β*-IEPOX solution
321 in ethyl acetate in a glass bulb at room temperature (~23 °C), and was injected into the flow tube via a
322 movable injector downstream of the aerosol inlet. A constant 2 L min^{-1} flow of conditioned aerosol was
323 drawn through the flow tube by the CIMS and a scanning mobility particle sizer (SMPS) connected to the
324 flow tube exit, which provided real-time measurements of the gas-phase IEPOX concentration and aerosol
325 surface area (Sa), respectively. The IEPOX injector was moved in 10 cm increments from the bottom (10
326 cm above the flow exit) to the top (70 cm above the flow exit) of the flow tube to vary the reaction time
327 between IEPOX and aerosol particles. The decay of gas phase IEPOX signal versus injector position
328 (reaction time) in the presence and absence of aerosol particles was measured to derive k_{obs} and k_{wall},
329 respectively, and the pseudo-first-order reaction rate constant k_{het} for IEPOX uptake onto particles was
330 determined as $k_{het} = k_{obs} - k_{wall}$. The IEPOX signals measured at every three adjacent injector positions (i.e.,

10-30, 20-40, 30-50, 40-60, 50-70 cm), which correspond to different average reaction times, were used to determine the k_{het} and then γ_{IEPOX} as a function of reaction time. γ_{IEPOX} is calculated by the following equation:

$$\gamma_{IEPOX} = \frac{4k_{het}}{S_a \omega} \quad (7)$$

where ω is the mean molecular speed of *trans*-β-IEPOX under the experimental condition (ω_{IEPOX}=231 m s^{-1}).[13,14]

Viscosity Calculation of IEPOX-derived OS and water mixtures. The improved parameterization by Derieux et al.[15] was designed to predict, Tg of pure compounds containing carbon, hydrogen and oxygen using the number of carbon (nC), hydrogen (nH), and oxygen (nO), as shown in eqn. 8.

$$T_{g,org} = \frac{n_C^0 + \ln(n_C)}{b_C} + \ln(n_H) b_H + \ln(n_C) \ln(n_H) b_{CH} + \ln(n_O) b_O + \ln(n_C) \ln(n_O) b_{CO} \quad (8)$$

where n_C^0 is the reference carbon number, b_C, b_H and b_O represent the contribution of each atom to T_g, and b_{CH} and b_{CO} are coefficients that reflect contributions from carbon–hydrogen and carbon–oxygen bonds, respectively. The values for these parameters used in this study were derived by DeRieux et al.[15] based on empirical fit and are shown in Table S6. However, the sulfur atom was not considered in the method. For a conservative estimation of T_g of IEPOX-OS, the sulfur atom is assumed to have the same effect on T_g as an oxygen atom. The T_g of IEPOX-OS, IEPOX-OS dimer and trimer are estimated to be 298 K, 333 K, and 360 K, respectively. The glass transition temperature of the sum of uncharacterized IEPOX-derived OS is assumed to be the same as the IEPOX-OS dimers to give a more conservative estimation. Taking into account the mass fraction of each OS compound based on the chemical data shown in Figure 1B (Amazon ratio) at 120 min, the T_g of the IEPOX-OS mixtures is calculated using the Gordon-Taylor equation based on the estimation of hygroscopicity, and the Gordon-Taylor constant among orgnaic compounds (k_{GT}=1) as well as the Gordon-Taylor constant between water and the organics (k_{GT}=12.5), as shown in eqn. 9. The upper hygroscospity value of 0.15 is based on the upper hygroscopicity range of organic compounds.

Gordon-Tayler constants between IEPOX-OS mixtures and water, and IEPOX-OS mixtures themselves are assumed to be 2.5, and 1, respectively based on previous studies.[15–18]

$$T_{g,\,mix}(RH) = \frac{(1 - w_{org}(RH))T_{g,c} + \frac{1}{k_{GT}}\sum_{i=1}^{n} w_{i,org}(RH)\, T_{g,i,org}}{(1 - w_{org}(RH)) + \frac{1}{k_{GT}}\sum_{i=1}^{n} w_{i,org}(RH)} \qquad (9)$$

where n denotes total number of organic compounds in the mixture and i denotes each organic compound; w_(i,org) is the mass fraction of organic compound i. The dependency of viscosity on RH is reflected in mass fraction terms as variable RH changes the amount of water taken up by the SOA, which can be calculated using hygroscopicity (κ).[15,19]

Thermodynamic Model of Aerosol pH.

The pH of aerosol particles during the reaction processes are calcualted using a termodynamic model employing two methods. The first method uses measured SO_4^{2-} concentration as well as the NH_4^+ concentration at the beginning of the experiment as the input values. The IEPOX-OS concentration was not considered. The second method takes into consideration all cations and anions in the aqueous aerosol particle.

The acidity model considers the acid disassociation of NH_4HSO_4 and H_2O. For scenario 1, the IEPOX-OSs were not considered. For scenario 2, IEPOX-OSs, including IEPOX-OS, IEPOX-OS dimer, and IEPOX-OS trimer, were taken into consideration in the model. The acid disassociation reactions of the above compounds are described below:

$$NH_4 + H_2O \rightleftharpoons NH_3 \cdot H_2O + H^+ \qquad (10)$$

$$HSO_4^- \rightleftharpoons H^+ + SO_4^{2-} \qquad (11)$$

$$H_2O \rightleftharpoons H^+ + OH^- \qquad (12)$$

$$IEPOX - OS \rightleftharpoons IEPOX - OS^- + H^+ \qquad (13)$$

$$IEPOX - OS_{dimer} \rightleftharpoons IEPOX - OS_{dimer}^- + H^+ \qquad (14)$$

$$IEPOX - OS_{trimer} \rightleftharpoons IEPOX - OS_{trimer}^- + H^+ \qquad (15)$$

The acid disassociation equilibrium equations for (10)-(15) were constructed, with pK_a values for Eqs. (7,8,9) were obtained from the literature. The pK_a values for Eqs. (13)-(15) were assumed to be ~2, with a range of 0-4. The proton balance equation together with the mass balance equations for NH_4^+, HSO_4^-, H^+, SO_4^{2-}, and IEPOX-OS monomer, dimer, and trimers were built to solve the H^+ ion concentration. The gas-particle balance of the NH_3, NH_4^+ was considered with a Henry's law constant of 0.0161 atm M^{-1}. A growth factor of 1.3 was used to calculate the liquid water content of the particles. The activity coefficients for all ions were assumed to be 1.

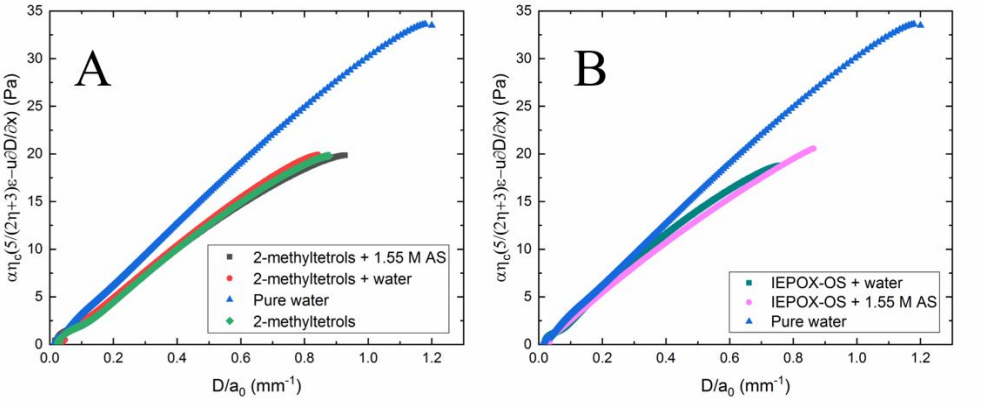

386

387 **Figure S1.** Representative Taylor plots (single droplet) for (A) 2-MT and (B) IEPOX-OS samples (in
388 water). The slope of the linear portion of the curves is equal to the interfacial tension. Interfacial tensions
389 reported in this work are the median values of interfacial tension (over all droplets) for any given system.
390 Normalized data points are shown in Figures 4A and S3.

391

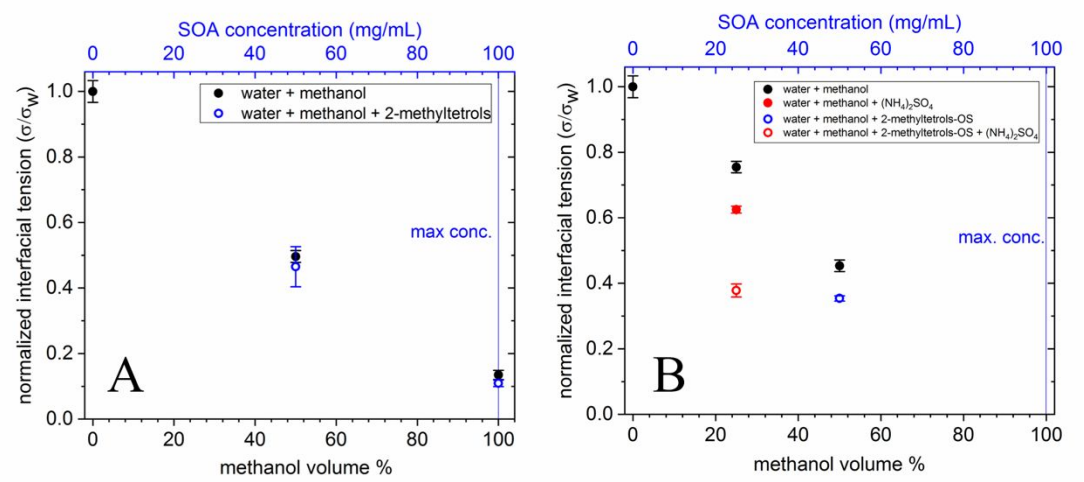

392

393 **Figure S2.** Interfacial tensions measured with microfluidics, for (A) 2-MT and (B) IEPOX-OS, with
394 methanol as the solvent. For 2-MT, approximately 300 µL of sample was used to prepare a 50 mg/mL
395 sample of 2-MT in water, approximately 300 µL was used to prepare a 50 mg/mL solution with AS and the
396 remaining was used for the 100 mg/mL experiment. Similarly, two different solutions were prepared for
397 the IEPOX-OS measurements (with and without AS) at 50 mg/mL.

398

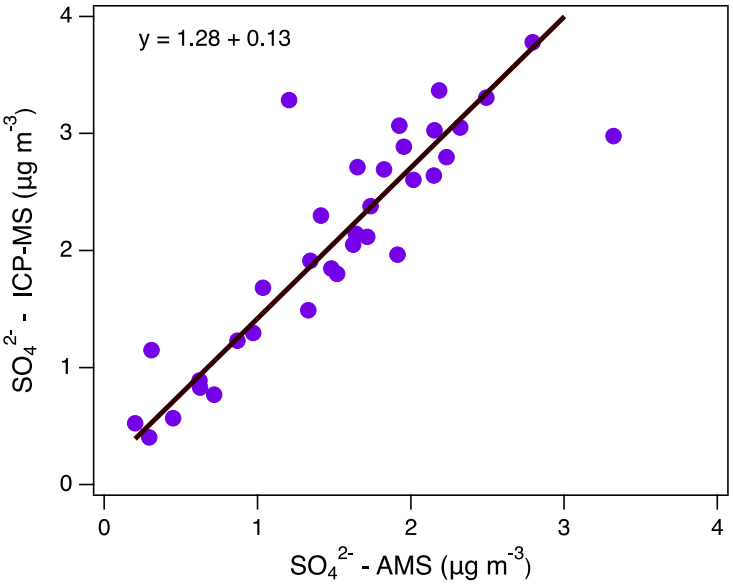

399

400 **Figure S3**. Comparison between aerosol sulfate measured by ICP-MS and AMS during the campaign in
401 the SE-U.S.

402

403

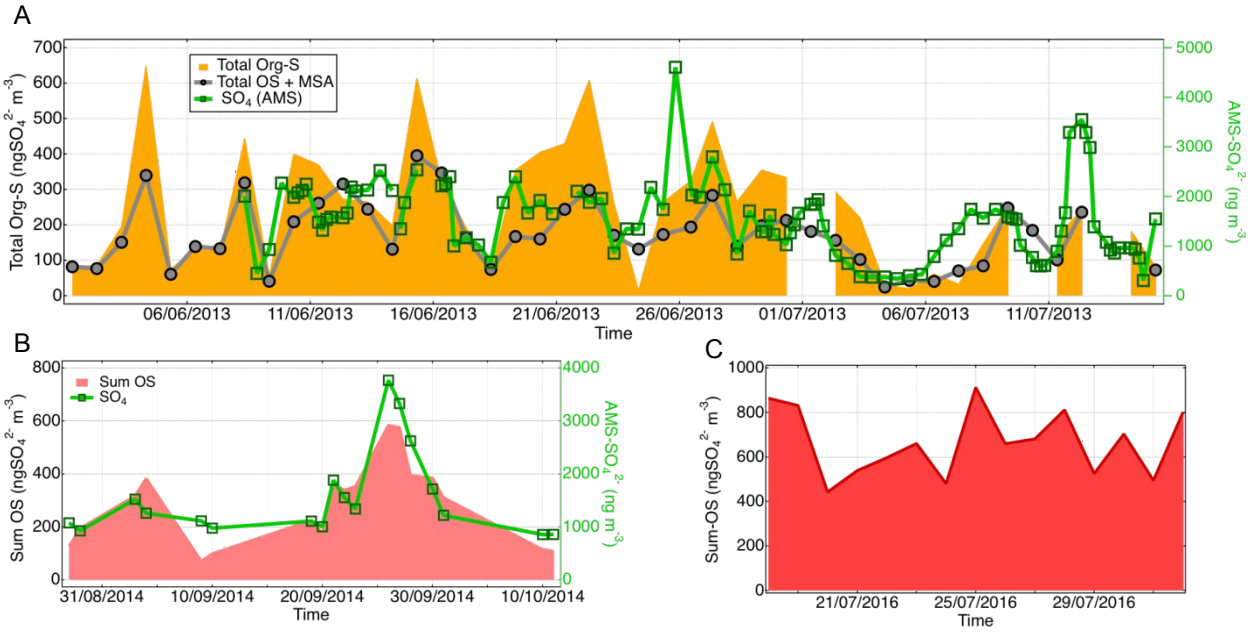

404

405 **Figure S4.** (A) Time-series of the sum of identified OS + MSA and total organosulfur compounds (Org-S)
406 quantified by UPLC/ESI-HR-Q-TOFMS and IR-ICP-MS, respectively, in the $PM_{2.5}$ samples collected
407 during the 2013 SOAS campaign. (B) and (C) present the concentrations of the sum of OS + MSA
408 quantified in downwind Manaus and Manaus, respectively.

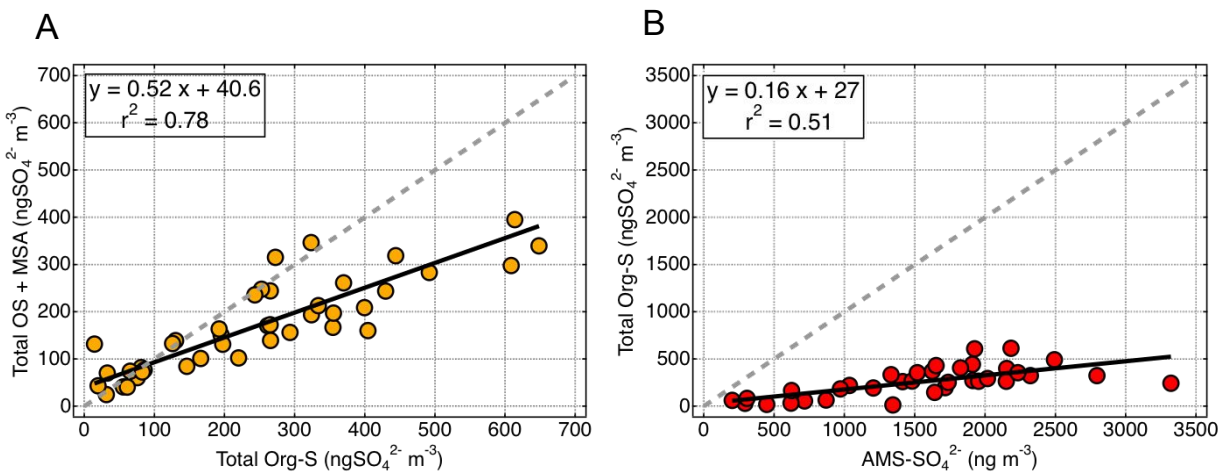

409

410 **Figure S5.** (A) Correlation between the sum of OS + MSA (y-axis) and Org-S (x-axis). This correlation
411 suggests significant unidentified sources of organosulfur compounds in SOA sampled in the SE-U.S. (B)
412 Correlation between Org-S (y-axis) and the mass of sulfate measured by the AMS in SE-US. Dashed grey
413 lines correspond to 1:1 line. OS + MSA were quantified by UPLC/ESI-HR-Q-TOFMS, and Org-S were
414 quantified by IR-ICP-MS.

415

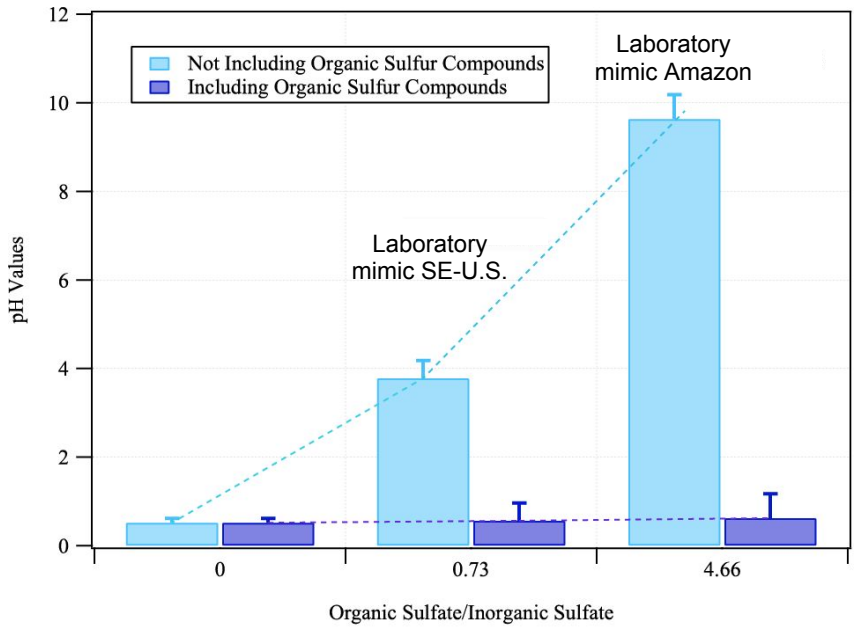

Figure S6. Comparison of modeled aerosol pH when considering the acidity of IEPOX-OS vs. not considering IEPOX-OS. The x axis is the ratio of the total organic sulfur compounds vs. total inorganic sulfur compounds in the aerosol. The light blue bars represent the modelling results of the chamber data without considering IEPOX-OS. The purple bars represent is the modeling results after taking IEPOX-OS into consideration. The center and the right groups show the modelled pH based on aerosol composition measured at the end of the experiment from the SE-U.S. ratio and the Amazon ratio chamber experiments, respectively. The error bar range is calculated based on the pKa values of IEPOX-OS to be 0-4. The dashed lines are trendlines. A growth factor of 1.3 and Henry's law constant for 0.0161 atm M^{-1} are applied in the model. By varying the pK_a values of IEPOX-OS, the aerosol acidity changes up to 6 times (0.8 pH units), suggesting the importance of further research on the role of these SOA constituents in governing the aerosol acidity.

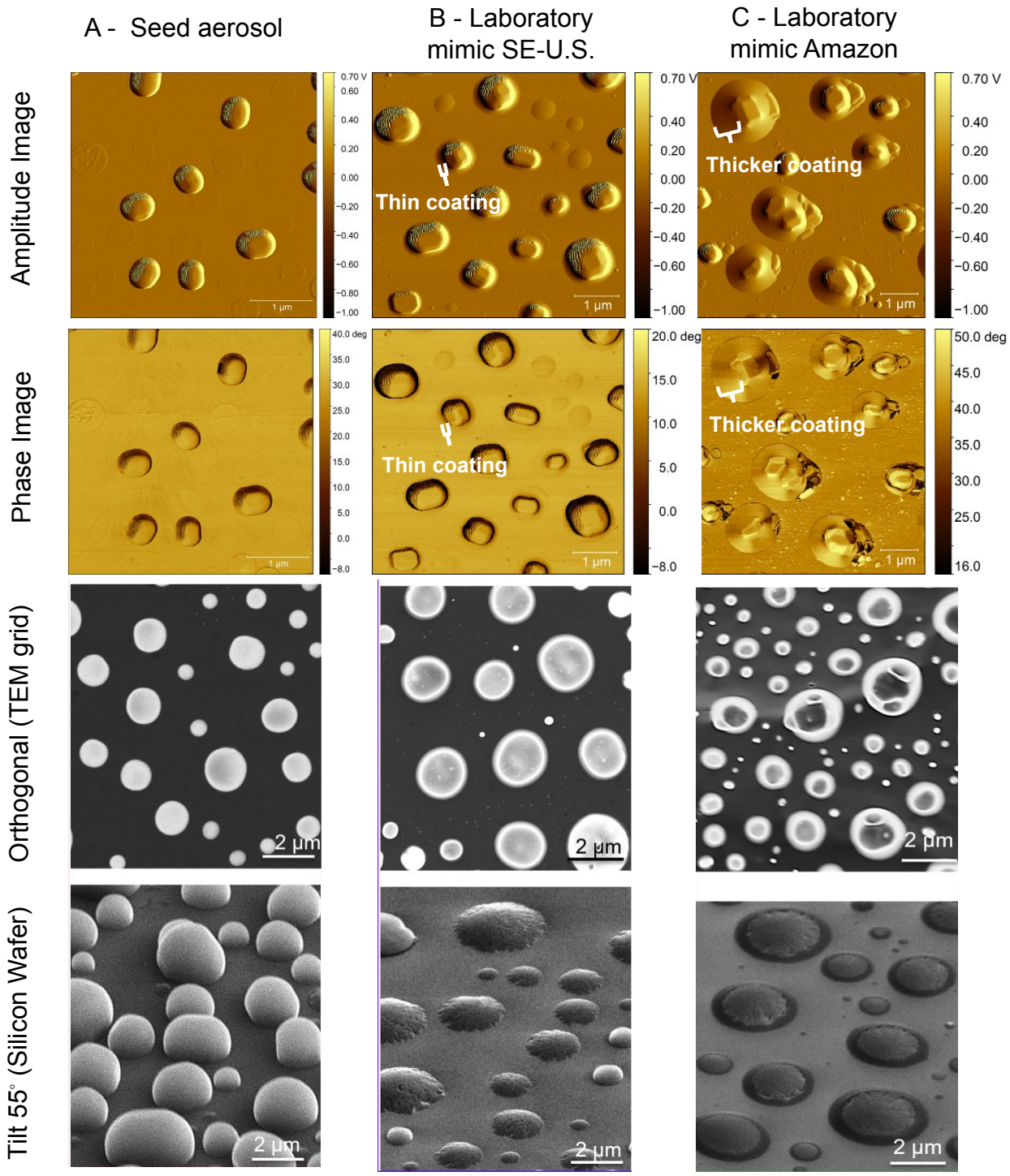

Figure S7. AFM phase and amplitude images for the corresponding height images shown in Figure 3. Scanning electron microscopy images on TEM grids orthogonal to the electron beam (top) and at a 55 degree tilt from the beam for (A) seed aerosol, (B) laboratory mimic SE-U.S. conditions and (C) laboratory mimic Amazon conditions (green). SE-U.S. and Amazon are after exposure to IEPOX.

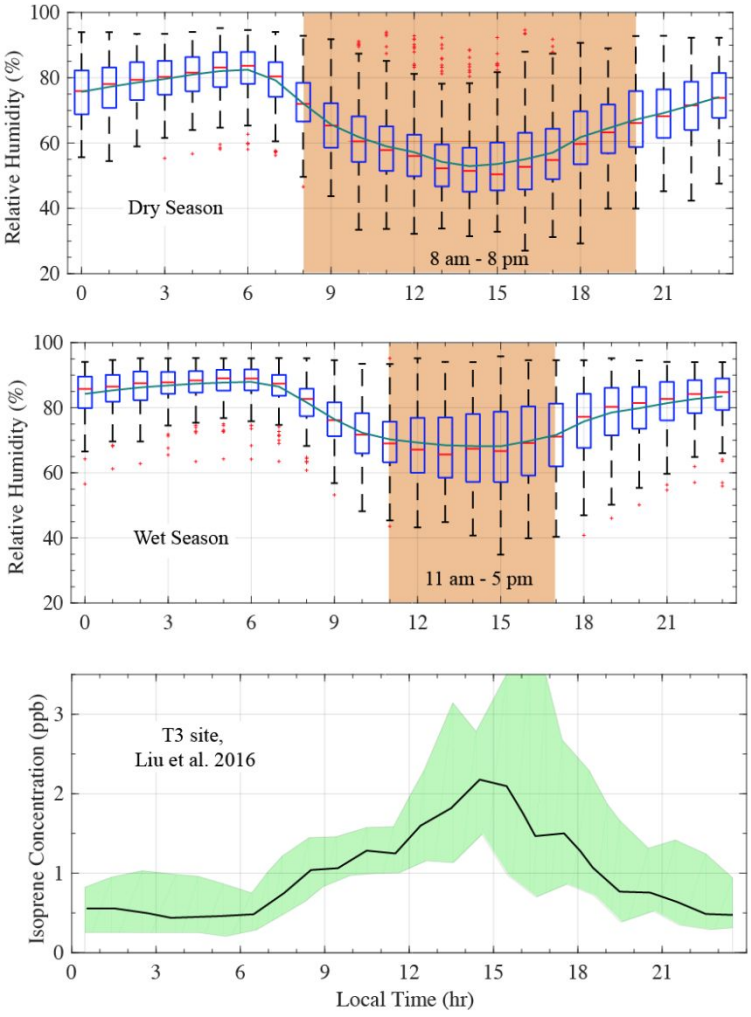

Figure S8. The top two panels show the box plots of the hourly relative humidity during dry season (June-September) and wet season (December-March) from 2016-2018 at the Amazon basin (Manaus site). On each box, the central mark indicates the median, and the bottom and top edges of the box indicate the 25th and 75th percentiles, respectively. The whiskers extend to the most extreme data points not considered outliers, and the outliers are shown individually with red plus symbols. Boxplot assigns points as outliers if they are greater than $q_3 + 1.5 \times (q_3 - q_1)$ or less than $q_1 - 1.5 \times (q_3 - q_1)$, where q_1 and q_3 are the 25th and 75th percentiles of the sample data, respectively. The black line in the bottom panel shows the measured hourly isoprene concentration downwind Manaus in the Amazon basin [20]. For the stations, hourly RH values (calculated from measured temperature and dew point) were retrieved from NOAA's National Climatic Data Center (http://www.ncdc.noaa.gov/). The green lines in the top two panels represent the mean hourly RH. The orange-shaded areas represent the periods when the average RH<70%.

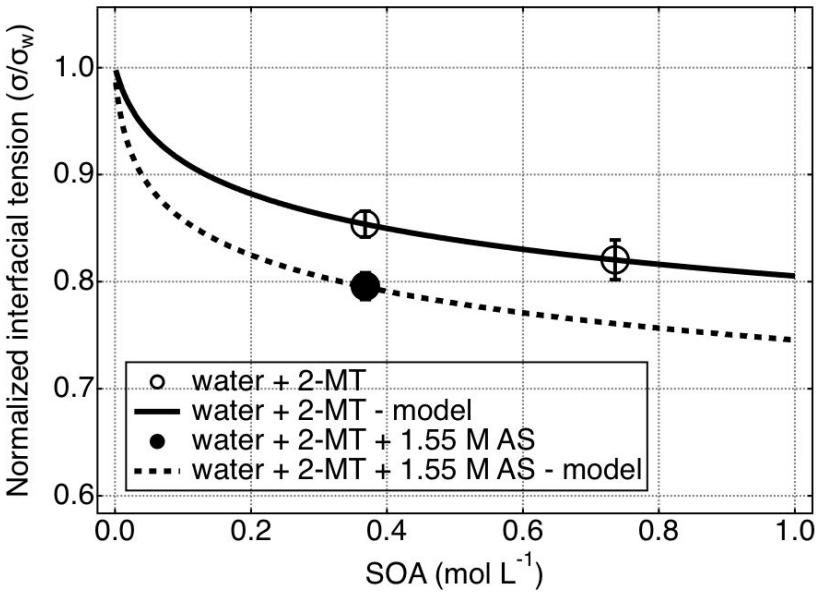

446

447 **Figure S9.** Measured and modeled interfacial tensions for 2-methyltetrols (2-MT).

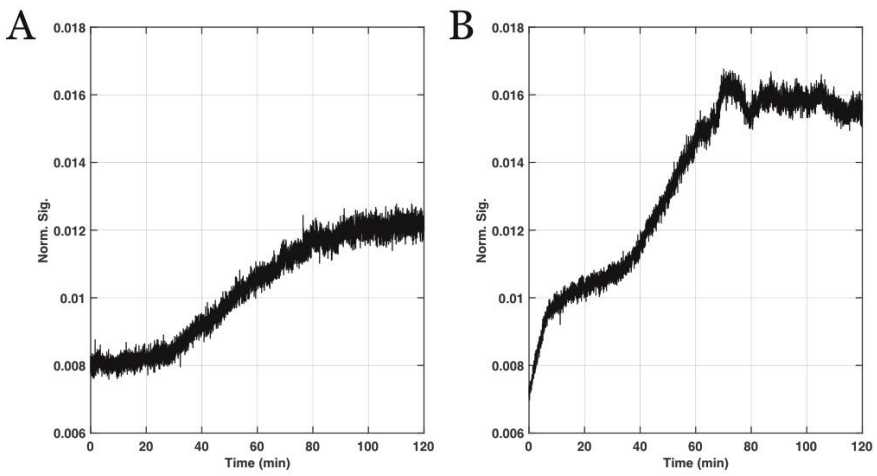

Figure S10. Time series of IEPOX signal in aerosol particles normalized by iodide signal measured by a high-resolution time-of-flight chemical ionization mass spectrometer equipped with iodide (I^-) reagent ion chemistry (I-HR-TOF-CIMS) during the reactive uptake of IEPOX chamber experiments under atmospheric IEPOX:SO_4^{2-} relevant to (A) SE-U.S. and (B) Amazon, corresponding to experiments shown in Figures 1A & 1B, respectively. Increasing slope of IEPOX signal indicates the injection rate of IEPOX was faster than its reactive and wall losses, a decreasing slope indicates reactive uptake to the particle phase is gradually slowing down as the reaction continues.

Table S1. Summary of indoor smog chamber conditions used for IEPOX uptake experiments using ammonium bisulfate (ABS) seed aerosols.

No	Description	Injected IEPOX (ppb)	SO_4^{2-} (μg/m^3)	IEPOX/SO_4	RH (%)
1	IEPOX + ABS	48	430.2	0.5	49.8
2	IEPOX + ABS	104	658.4	0.8	47.0
3	IEPOX + ABS	122	664.0	0.9	46.3
4	IEPOX + ABS	172	669.6	1.3	53.2
5	IEPOX + ABS	140	437.4	1.5	52.2
6	IEPOX + ABS	166	179.2	4.5	48.9
7	IEPOX + ABS	218	175.8	6.0	47.7
8	IEPOX + ABS	240	111.1	10.5	48.9
9	IEPOX + ABS	174	76.4	11.1	46.4
10	IEPOX + ABS	176	70.7	12.1	48.0
11	IEPOX + ABS	230	65.6	17.1	50.4
12	IEPOX + ABS	124	31.0	19.5	46.5
13	IEPOX + ABS	174	41.1	20.7	48.8

460 **Table S2.** Average and maximum concentrations of the OS identified during the 2013 SOAS campaign.

Suggested Formula	$[M-H]^-$ ion	Average concentration (ng m^{-3})	Max concentration (ng m^{-3})	Average OS/Sum OS (%)	Precursor group
$CH_3O_3S^-$ [a,b]	94.98	39.27	167.59	10.53	Dimethylsulfide
$CH_3O_4S^-$ [a,c]	110.97	3.03	20.95	0.82	-
$C_2H_3O_5S^-$ [a,c]	138.97	0.83	2.51	0.26	Isoprene / Anthropogenic
$C_3H_5O_5S^-$ [a,c]	152.98	4.95	18.22	1.34	Isoprene / Anthropogenic
$C_3H_5O_6S^-$ [a,c]	168.98	12.83	35.33	3.10	Isoprene / Anthropogenic
$C_5H_9O_5S^-$ [a,d]	181.01	0.14	2.51	0.04	Isoprene
$C_4H_7O_6S^-$ [a,c]	182.99	8.60	23.51	2.30	Isoprene
$C_5H_9O_6S^-$ [a,e]	197.01	4.79	16.87	0.74	Isoprene
$C_4H_7O_7S^-$ [a,d]	198.99	10.72	43.07	2.90	Isoprene
$C_5H_{11}O_6S^-$ [a,e]	199.02	2.78	9.04	0.73	Isoprene
$C_8H_9O_4S^-$ [a,e]	201.02	1.39	4.17	0.37	Isoprene
$C_5H_7O_7S^-$ [a,e]	210.99	7.31	27.45	1.96	Isoprene
$C_5H_9O_7S^-$ [a,e]	213.00	7.84	23.99	2.10	Isoprene
$C_5H_{11}O_7S^-$ [a,e]	215.02	217.14	755.3	58.39	Isoprene
$C_5H_7O_8S^-$ [a,e]	226.98	4.25	14.12	1.14	Isoprene
$C_6H_{11}O_7S^-$ [a,e]	227.02	0.43	2.94	0.11	Isoprene
$C_5H_9O_8S^-$ [a,e]	229.00	6.91	21.33	1.82	Isoprene
$C_5H_{11}O_8S^-$ [a,e]	231.01	0.38	3.72	0.12	Isoprene
$C_7H_{11}O_7S^-$ [f,g]	239.02	4.20	14.22	1.29	Limonene
$C_{10}H_{17}O_5S^-$ [f,h]	249.08	0.93	2.56	0.26	Monoterpenes

Suggested Formula	$[M-H]^-$ ion	Average concentration (ng m^{-3})	Max concentration (ng m^{-3})	Average OS/Sum OS (%)	Precursor group
$C_5H_{10}NO_9S^{-}$ [f,g]	260.00	16.41	124.14	4.40	Isoprene
$C_9H_{15}O_7S^{-}$ [f,h]	267.05	1.39	3.36	0.37	Isoprene / Limonene
$C_{10}H_{15}O_7S^{-}$ [f,h]	279.05	1.02	3.41	0.30	Monoterpenes
$C_{10}H_{17}O_7S^{-}$ [f,h]	281.07	2.15	15.10	0.60	α-terpinene
$C_{10}H_{16}NO_7S^{-}$ [f,h]	294.06	4.24	88.69	1.17	Monoterpenes
$C_9H_{14}NO_8S^{-}$ [f,h]	296.04	0.53	6.76	0.15	Limonene
$C_{10}H_{16}NO_8S^{-}$ [f,h]	310.06	12.88	96.11	3.47	Monoterpenes
$C_{10}H_{19}O_9S^{-}$ [f,h]	315.07	0.36	1.44	0.19	Isoprene
$C_{10}H_{14}NO_9S^{-}$ [f,h]	324.04	1.12	13.56	0.31	Monoterpenes
$C_{10}H_{16}NO_9S^{-}$ [f,h]	326.05	1.47	15.89	0.41	Monoterpenes
$C_{10}H_{21}O_{10}S^{-}$ [f,g]	333.08	0.69	3.23	0.18	Isoprene
$C_{10}H_{16}NO_{10}S^{-}$ [f,h]	342.05	0.31	2.12	0.09	Monoterpenes
$C_{10}H_{15}N_2O_{10}S^{-}$ [f,h]	355.04	0.81	18.66	0.22	α-pinene
$C_{10}H_{17}N_2O_{11}S^{-}$ [f,h]	373.06	0.34	7.17	0.10	Limonene

[a] OS are eluted within the first 2 minutes; [b] quantified using methylsulfonic acid; [c] OS quantified using 2-oxopropyl sulfate; [d] OS quantified using 2-methylglyceric acid sulfates; [e] OS quantified using 2-methyltetrol sulfates; [f] OS are eluted during the elution gradient; [g] OS quantified using propyl sulfate; [h] OS quantified using 3-pinanol-2-hydrogen sulfate; [i] OS quantified using octyl sulfate.

468 **Table S3.** Average and maximum concentrations of the OS identified during the Go-Amazon
469 campaign.

Suggested Formula	$[M-H]^-$ ion	Average concentration (ng m^{-3})	Max concentration (ng m^{-3})	Average OS/Sum OS (%)	Precursor group
$C_3H_5O_5S^-$ [a,b]	152.98	29.9	69.6	4.8	Isoprene / Anthropogenic
$C_3H_5O_5S^-$ [a,b]	154.98	25.3	47.9	4.1	Isoprene / Anthropogenic
$C_3H_5O_6S^-$ [a,b]	168.98	19	45.6	1.4	Isoprene / Anthropogenic
$C_4H_7O_6S^-$ [a,b]	182.99	29.5	71.4	3.1	Isoprene
$C_5H_{11}O_6S^-$ [a,b]	199.02	101.0	283.4	16.3	Isoprene
$C_5H_{11}O_7S^-$ [a,b]	215.02	398.5	1450.2	64.2	Isoprene

470 [a] *OS are eluted within the first 2 minutes;* [b] *OS quantified using 2-methyltetrol sulfates*.
471

472 **Table S4.** Average and maximum concentrations of the OS identified in Manaus.

Suggested Formula	$[M-H]^-$ ion	Average concentration (ng m^{-3})	Max concentration (ng m^{-3})	Average OS/Sum OS (%)	Precursor group
$C_2H_3O_5S^-$ [a,c]	138.97	19.8	25.2	1.3	Isoprene / Anthropogenic
$C_3H_5O_5S^-$ [a,c]	152.98	87.4	301.1	5.8	Isoprene / Anthropogenic
$C_3H_5O_5S^-$ [a,c]	154.98	87.0	122.8	5.8	Isoprene / Anthropogenic
$C_5H_7O_5S^-$ [f,g]	179.0	4.0	11.9	0.3	Cyclohexene
$C_4H_7O_6S^-$ [a,c]	182.99	47.1	120.7	3.1	Isoprene
$C_6H_{11}O_5S^-$ [f,g]	195.03	1.5	7.0	0.1	Cyclohexene/ Pinonaldehyde
$C_5H_9O_6S^-$ [a,e]	197.01	15.6	24.5	1.0	Isoprene
$C_5H_{11}O_6S^-$ [a,e]	199.02	58.9	84.2	3.9	Isoprene
$C_5H_7O_7S^-$ [a,e]	210.99	9.7	13.8	0.6	Isoprene
$C_5H_9O_7S^-$ [a,e]	213.00	100.5	137.8	6.7	Isoprene
$C_5H_{11}O_7S^-$ [a,e]	215.02	823.3	1159.7	55.0	Isoprene
$C_7H_{11}O_5S^-$ [f,g]	223.02	6.5	11.2	0.4	α-pinene
$C_5H_9O_8S^-$ [a,e]	229.00	20.1	27.1	1.3	Isoprene
$C_5H_{11}O_8S^-$ [a,e]	231.01	7.0	9.7	0.5	Isoprene
$C_7H_{11}O_7S^-$ [f,g]	237.04	6.1	8.3	0.4	α-pinene
$C_7H_{11}O_7S^-$ [f,g]	239.02	14.5	19.2	1.0	Limonene
$C_{10}H_{17}O_5S^-$ [f,h]	249.04	24.1	69.4	1.6	Monoterpenes
$C_{10}H_{19}O_5S^-$ [f,h]	251.09	7.6	19.7	0.5	Cyclodecane
$C_8H_{13}O_7S^-$ [f,g]	253.03	3.4	4.7	0.2	Isoprene

Suggested Formula	$[M-H]^-$ ion	Average concentration (ng m^{-3})	Max concentration (ng m^{-3})	Average OS/Sum OS (%)	Precursor group
$C_5H_{10}NO_7S^{-}$ [f,g]	260.00	48.7	19.2	0.6	Isoprene
$C_{10}H_{15}O_7S^{-}$ [f,h]	279.05	9.6	13.9	0.6	Monoterpene
$C_{12}H_{23}O_5S^{-}$ [f,i]	279.12	6.3	10.9	0.4	Dodecane
$C_{10}H_{17}O_7S^{-}$ [f,h]	281.06	13.8	22.7	0.9	Monoterpene
$C_{10}H_{16}NO_7S^{-}$ [f,h]	295.06	39.0	56.0	2.6	Monoterpene
$C_9H_{14}NO_8S^{-}$ [f,h]	296.04	2.7	5.9	0.2	Limonene
$C_{10}H_{19}O_{10}S^{-}$ [f,h]	331.06	16.5	26.7	1.1	Isoprene
$C_{10}H_{21}O_{10}S^{-}$ [f,h]	333.08	50.1	90.6	3.3	Isoprene
$C_{20}H_{39}O_{15}S^{-}$ [f,g]	451.14	1.8	5.5	0.1	Isoprene

[a] OS are eluted within the first 2 minutes; [b] quantified using methylsulfonic acid; [c] OS quantified using 2-oxopropyl sulfate; [d] OS quantified using 2-methylglyceric acid sulfates; [e] OS quantified using 2-methyltetrol sulfates; [f] OS are eluted during the elution gradient; [g] OS quantified using propyl sulfate; [h] OS quantified using 3-pinanol-2-hydrogen sulfate; [i] OS quantified using octyl sulfate.

Table S5. Calibration factors and retention times of the OS standards.

Formula	Name	$[M-H]^-$	Calibration factor	r^2	Retention time(s) (min)
$C_4H_7O_7S^-$	2-methylglyceric acid sulfate	198.99	1.01×10^6	0.99	1.8
$C_5H_{11}O_7S^-$	2-methyltetrol sulfate	215.02	1.02×10^6	0.99	1.1/1.8
$C_2H_3O_6S^-$	Glycolic acid sulfate	154.96	1.09×10^6	0.98	1.8
$C_3H_5O_5S^-$	2-oxopropyl sulfate	152.98	1.16×10^6	0.99	1.8
$C_3H_7O_4S^-$	Propyl sulfate	139.00	3.68×10^6	0.99	3.5
$C_9H_{13}O_6S^-$	3-pinanol-2-hydrogen sulfate	249.04	3.01×10^6	0.90	8.6
$C_8H_{17}O_4S^-$	Octyl sulfate	209.08	1.10×10^8	0.99	11.5

Table S6. The fitting parameters for the glass transition calculation at dry condition.

n_C^0	b_C	b_H	b_{CH}	b_O (b_S)	b_{CO}
12.13	10.95	-41.82	21.61	118.96	-24.38

Table S7. Parameters Used for the Viscosity Calculation of IEPOX-derived OS. Values in the parathesis represent the upper and lower bound values.

Compound	Glass Transition Temperature of Dry SOA ($T_{g,org}$) (K)	Hygroscopicity (κ)	Fragility (D)	The Gordon–Taylor Constant (k_{GT}):
α-Pinene SOA	278.5 (268.5-300)	0.1 (0.1)	10 (10-20)	2.5 (2.5-3.0)
2-Methyltetrol Sulfate	298 (288-320)	0.12 (0.1-0.15)	13 (10-20)	2.5 (2.5-3.0)
IEPOX-derived OS Mixture	313 (303-330)	0.12 (0.1-0.15)	13 (10-20)	2.5 (2.5-3.0)

References Supplementary Materials.

(1) Budisulistiorini, S. H.; Li, X.; Bairai, S. T.; Renfro, J.; Liu, Y.; Liu, Y. J.; McKinney, K. A.; Martin, S. T.; McNeill, V. F.; Pye, H. O. T.; Nenes, A.; Neff, M. E.; Stone, E. A.; Mueller, S.; Knote, C.; Shaw, S. L.; Zhang, Z.; Gold, A.; Surratt, J. D. Examining the Effects of Anthropogenic Emissions on Isoprene-Derived Secondary Organic Aerosol Formation during the 2013 Southern Oxidant and Aerosol Study (SOAS) at the Look Rock, Tennessee Ground Site. *Atmospheric Chemistry and Physics* **2015**, *15* (15), 8871–8888. https://doi.org/10.5194/acp-15-8871-2015.

(2) Martin, S. T.; Artaxo, P.; Machado, L. A. T.; Manzi, A. O.; Souza, R. A. F.; Schumacher, C.; Wang, J.; Andreae, M. O.; Barbosa, H. M. J.; Fan, J.; Fish, G.; Goldstein, A. H.; Guenther, A.; Jimenez, J. L., Pöschl, U.; Silva Dias, M. A.; Smith, J. N.; Wendisch M. Introduction: Observations and Modeling of the Green Ocean Amazon (GoAmazon2014/5). *Atmospheric Chemistry and Physics* **2016**, *16* (8), 4785–4797. https://doi.org/10.5194/acp-16-4785-2016.

(3) Liu, P.; Li, Y. J.; Wang, Y.; Gilles, M. K.; Zaveri, R. A.; Bertram, A. K.; Martin, S. T. Lability of Secondary Organic Particulate Matter. *Proceedings of the National Academy of Sciences* **2016**, *113* (45), 12643–12648. https://doi.org/10.1073/pnas.1603138113.

(4) Lin, Y.-H.; Budisulistiorini, S. H.; Chu, K.; Siejack, R. A.; Zhang, H.; Riva, M.; Zhang, Z.; Gold, A.; Kautzman, K. E.; Surratt, J. D. Light-Absorbing Oligomer Formation in Secondary Organic Aerosol from Reactive Uptake of Isoprene Epoxydiols. *Environmental Science & Technology* **2014**, *48* (20), 12012–12021. https://doi.org/10.1021/es503142b.

(5) Riva, M.; Budisulistiorini, S. H.; Chen, Y.; Zhang, Z.; D'Ambro, E. L.; Zhang, X.; Gold, A.; Turpin, B. J.; Thornton, J. A.; Canagaratna, M. R.; Surratt, J. D. Chemical Characterization of Secondary Organic Aerosol from Oxidation of Isoprene Hydroxyhydroperoxides. *Environmental Science & Technology* **2016**, *50* (18), 9889–9899. https://doi.org/10.1021/acs.est.6b02511.

(6) Rattanavaraha, W.; Chu, K.; Budisulistiorini, S. H.; Riva, M.; Lin, Y.-H.; Edgerton, E. S.; Baumann, K.; Shaw, S. L.; Guo, H.; King, L.; Weber, R. J.; Neff, M. E.; Stone, E. A.; Offenberg, J. H.; Zhang, Z.; Gold, A.; Surratt, J. D. Assessing the Impact of Anthropogenic Pollution on Isoprene-Derived Secondary Organic Aerosol Formation in $PM_{2.5}$ Collected from the Birmingham, Alabama, Ground Site during the 2013 Southern Oxidant and Aerosol Study. *Atmospheric Chemistry and Physics* **2016**, *16* (8), 4897–4914. https://doi.org/10.5194/acp-16-4897-2016.

(7) Riva, M.; Budisulistiorini, S. H.; Zhang, Z.; Gold, A.; Surratt, J. D. Chemical Characterization of Secondary Organic Aerosol Constituents from Isoprene Ozonolysis in the Presence of Acidic Aerosol. *Atmospheric Environment* **2016**, *130*, 5–13. https://doi.org/10.1016/j.atmosenv.2015.06.027.

(8) von Glasow, R.; Crutzen, P. J. Model Study of Multiphase DMS Oxidation with a Focus on Halogens. *Atmospheric Chemistry and Physics* **2004**, *4* (3), 589–608. https://doi.org/10.5194/acp-4-589-2004.

(9) Hettiyadura, A. P. S.; Jayarathne, T.; Baumann, K.; Goldstein, A. H.; de Gouw, J. A.; Koss, A.; Keutsch, F. N.; Skog, K.; Stone, E. A. Qualitative and Quantitative Analysis of Atmospheric Organosulfates in Centreville, Alabama. *Atmospheric Chemistry and Physics* **2017**, *17* (2), 1343–1359. https://doi.org/10.5194/acp-17-1343-2017.

(10) Schwier, A. N.; Viglione, G. A.; Li, Z.; Faye McNeill, V. Modeling the Surface Tension of Complex, Reactive Organic–Inorganic Mixtures. *Atmos. Chem. Phys.* **2013**, *13* (21), 10721–10732. https://doi.org/10.5194/acp-13-10721-2013.

(11) Toivola, M.; Prisle, N. L.; Elm, J.; Waxman, E. M.; Volkamer, R.; Kurtén, T. Can

534 COSMOTherm Predict a Salting in Effect? *The Journal of Physical Chemistry A* **2017**, *121* (33),
535 6288–6295. https://doi.org/10.1021/acs.jpca.7b04847.
536 (12) Gaston, C. J.; Riedel, T. P.; Zhang, Z.; Gold, A.; Surratt, J. D.; Thornton, J. A. Reactive
537 Uptake of an Isoprene-Derived Epoxydiol to Submicron Aerosol Particles. *Environmental Science*
538 *& Technology* **2014**, *48* (19), 11178–11186. https://doi.org/10.1021/es5034266.
539 (13) Zhang, Y.; Chen, Y.; Lambe, A. T.; Olson, N. E.; Lei, Z.; Craig, R. L.; Zhang, Z.; Gold,
540 A.; Onasch, T. B.; Jayne, J. T.; Worsnop, D. R.; Gaston, C. J.; Thornton, J. A.; Vizuete, W.; Ault,
541 A. P.; Surratt, J. D. Effect of the Aerosol-Phase State on Secondary Organic Aerosol Formation
542 from the Reactive Uptake of Isoprene-Derived Epoxydiols (IEPOX). *Environmental Science &*
543 *Technology Letters* **2018**, *5* (3), 167–174. https://doi.org/10.1021/acs.estlett.8b00044.
544 (14) Riedel, T. P.; Lin, Y.-H.; Budisulistiorini, S. H.; Gaston, C. J.; Thornton, J. A.; Zhang, Z.;
545 Vizuete, W.; Gold, A.; Surratt, J. D. Heterogeneous Reactions of Isoprene-Derived Epoxides:
546 Reaction Probabilities and Molar Secondary Organic Aerosol Yield Estimates. *Environmental*
547 *Science & Technology Letters* **2015**, *2* (2), 38–42. https://doi.org/10.1021/ez500406f.
548 (15) DeRieux, W.-S. W.; Li, Y.; Lin, P.; Laskin, J.; Laskin, A.; Bertram, A. K.; Nizkorodov, S.
549 A.; Shiraiwa, M. Predicting the Glass Transition Temperature and Viscosity of Secondary Organic
550 Material Using Molecular Composition. *Atmospheric Chemistry and Physics* **2018**, *18* (9), 6331–
551 6351. https://doi.org/10.5194/acp-18-6331-2018.
552 (16) Zobrist, B.; Marcolli, C.; Pedernera, D. A.; Koop, T. Do Atmospheric Aerosols Form
553 Glasses? *Atmospheric Chemistry and Physics* **2008**, *8* (17), 5221–5244.
554 https://doi.org/10.5194/acp-8-5221-2008.
555 (17) Koop, T.; Bookhold, J.; Shiraiwa, M.; Pöschl, U. Glass Transition and Phase State of
556 Organic Compounds: Dependency on Molecular Properties and Implications for Secondary
557 Organic Aerosols in the Atmosphere. *Physical Chemistry Chemical Physics* **2011**, *13* (43), 19238.
558 https://doi.org/10.1039/c1cp22617g.
559 (18) Dette, H. P.; Koop, T. Glass Formation Processes in Mixed Inorganic/Organic Aerosol
560 Particles. *The Journal of Physical Chemistry A* **2015**, *119* (19), 4552–4561.
561 https://doi.org/10.1021/jp5106967.
562 (19) Petters, M. D.; Kreidenweis, S. M. A Single Parameter Representation of Hygroscopic
563 Growth and Cloud Condensation Nucleus Activity. *Atmospheric Chemistry and Physics* **2007**, *7*
564 (8), 1961–1971. https://doi.org/10.5194/acp-7-1961-2007.
565 (20) Liu, Y.; Brito, J.; Dorris, M. R.; Rivera-Rios, J. C.; Seco, R.; Bates, K. H.; Artaxo, P.;
566 Duvoisin, S.; Keutsch, F. N.; Kim, S.; et al. Isoprene Photochemistry over the Amazon Rainforest.
567 *Proceedings of the National Academy of Sciences* **2016**, *113* (22), 6125–6130.
568 https://doi.org/10.1073/pnas.1524136113.
569